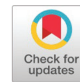

Dual ion beam grown silicon carbide thin films: Variation of refractive index and bandgap with film thickness

Aakash Mathur,[1] Dipayan Pal,[1] Ajaib Singh,[1] Rinki Singh,[2] Stefan Zollner,[3,4] and Sudeshna Chattopadhyay[1,2,5,a)]

[1]*Discipline of Metallurgy Engineering and Materials Science, Indian Institute of Technology Indore, Indore 453552, India*

[2]*Discipline of Biosciences and Biomedical Engineering, Indian Institute of Technology Indore, Indore 453552, India*

[3]*Department of Physics, New Mexico State University, Las Cruces, New Mexico 88003*

[4]*Institute of Physics, Academy of Sciences of the Czech Republic, Na Slovance 2, 182 21 Prague 8, Czech Republic*

[5]*Discipline of Physics, Indian Institute of Technology Indore, Indore 453552, India*

(Received 27 March 2019; accepted 10 June 2019; published 2 July 2019)

Amorphous SiC thin films on a silicon substrate (Si) with different film thicknesses (about 20–450 nm) were deposited using dual ion beam sputtering deposition (DIBSD) at room temperature. These SiC thin films were of high quality showing high coverage (>90%) and low surface and interface roughness (<5 Å). The structure and morphology of these SiC/Si systems were explored by x-ray reflectivity, x-ray diffraction, scanning electron microscopy, and atomic force microscopy. The bonding configuration and compositional details of the SiC films were examined by Fourier-transform infrared and Raman spectroscopy. The optical constants (complex dielectric function and refractive index) and the bandgap of SiC thin films were analyzed through spectroscopic ellipsometry in the 0.55–6.3 eV energy range. An increase in the bandgap (5.15–5.59 eV) and a corresponding decrease in the refractive index (2.97–2.77) were noticed with the increase of SiC film thickness from about 20–450 nm. This thickness dependent trend in optical properties is attributed to the increase of the C to Si atomic concentration ratio in DIBSD grown SiC thin films with increasing film thickness, as observed from energy dispersive x-ray analysis measurements. The unique properties of amorphous SiC have already placed it as a suitable candidate for solar cells and photovoltaic applications in its thin film form. The results developed in this study for thickness dependent optical properties of SiC thin films can be used for further optimizing the performance of SiC in various applications through tuning of optical properties. *Published by the AVS.* https://doi.org/10.1116/1.5097628

I. INTRODUCTION

Silicon carbide (SiC) is a superior wide and indirect bandgap semiconducting material with outstanding physical and chemical properties. Its physical properties such as high breakdown field, high saturated drift velocity, and high thermal conductivity make it a prime candidate and stable material for high temperature, high radiation tolerance, high voltage, high power, and high-frequency applications.[1,2] Silicon carbide exists in a large number of polytypes or structural forms, with different stacking sequences of tetrahedral Si and C layers.[3,4] The use of crystalline SiC (*c*-SiC) films on a Si substrate is very advantageous because it combines the excellent properties of SiC with the well-known Si technology.[5,6] However, *c*-SiC deposition requires high temperature (>1000 °C), which is a problem for conventional microelectronics processes and increases the cost of the hardware needed for its production and the final product. Intense research has been carried out on amorphous SiC (*a*-SiC) layers that have been recognized as a good substitute for crystalline SiC due to their excellent coefficient of thermal expansion that matches with silicon wafers, high carrier mobility, high conductivity, relatively good thermal, mechanical stabilities, etc.[7,8] Amorphous SiC is one of the most attractive and promising materials since its bandgap ranges from 1.8 to 2.6 eV or more when its carbon content in the material varies.[9] Each device incorporating SiC thin films may have different requirements such as optical bandgap, refractive index, surface, and interface roughness. The thickness of the thin film is an important factor affecting the optical and electrical properties. Studies showed that the thickness of SiC films is a key parameter for use as a window layer of solar cells where thicknesses ranging from 15 to 400 nm are of specific interest regarding optimization of device performance.[10,11] Amorphous SiC can be used effectively as a durable thermally stable surface passivation material for high-efficiency thin silicon photovoltaic applications.[12] Also, its application fields have been expanding into various optoelectronic devices such as photodetectors, x-ray sensors, and color sensors.[13,14] Therefore, it is interesting and important to elucidate the relationship between the SiC film thickness, the corresponding structure, and its optical properties from the viewpoint of its varied applications.

The techniques for deposition of SiC thin films are crucial for their versatile applications from mechanical to electrical

Note: This paper is part of the Conference Collection: 8th International Conference on Spectroscopic Ellipsometry 2019, ICSE.

[a)]Author to whom correspondence should be addressed: sudeshna@iiti.ac.in and chattopadhyay.sudeshna@gmail.com

to optoelectronic applications. Recently, plasma-assisted deposition methods have been used to grow SiC films such as plasma enhanced chemical vapor deposition,[15,16] electron cyclotron resonance,[17] and conventional physical vapor deposition methods (magnetron sputtering[18] and pulsed laser deposition[19]). However, these methods need a relatively high temperature that creates defects resulting from the high stress generated by the different thermal expansion coefficients between SiC and the substrate.[20] Thus, finding an inexpensive method for the synthesis of large-scale, homogenous, high-quality, SiC thin films at lower temperature has remained a challenge for many years. Dual ion beam sputtering deposition (DIBSD) is a thin film growth technique from a single target sputtering process. This technique offers numerous other advantages such as a uniform compositional distribution in the thin film, smooth surfaces, and a simple deposition process.[21] One advantage of the DIBSD system compared to conventional sputtering techniques is that it yields high-quality thin films with comparatively better uniformity and adhesion to the substrate.[22–25] Achieving better quality film through the DIBSD technique as compared to conventional sputtering techniques is completely based on its working principle. DIBSD is equipped with a radio frequency (RF) deposition ion source and a direct-current coupled assist ion source.[21,24,25] An RF deposition source, which is used for sputtering the material from the target, is widely used for deposition of oxides and semiconductors, whereas an assist ion source is employed to preclean the substrate surface before film deposition and to hinder three-dimensional island formation and remove weak dangling bonds during film deposition process, assisting in the reduction of columnar growth of thin films and thereby enhancing growth uniformity and film adhesion to the substrate.[21,24,25] Also, in ion beam sputter deposition, ion generation and acceleration (ion beam source), the generation of film-forming particles (target) and thin film growth (substrate) are spatially separated. Therefore, geometrical parameters (ion incidence angle and emission angle) in addition to ion beam parameters (ion species and ion energy) can be varied, which results in different energy distributions of the film-forming particles. The spatial separation also avoids interaction of the plasma, target, and substrate, which is inherent in magnetron sputtering (e.g., arcing).[26–28]

In this work, SiC thin films of varied thicknesses in the range of about 20–450 nm were grown by the DIBSD technique to study the thickness dependent optical properties corresponding to their internal structure. The structure and morphology of these films were analyzed through x-ray reflectivity (XRR), powder x-ray diffraction (XRD), scanning electron microscopy (SEM), and atomic force microscopy (AFM). Spectroscopic techniques such as Fourier-transform infrared (FTIR) and Raman scattering spectroscopy have also been employed to explore the bonding configuration and chemical composition of the SiC thin films with different thicknesses. The optical constants (real and imaginary parts of the complex dielectric function and refractive index) and bandgap of the thin films were estimated using spectroscopic ellipsometry (SE). Key attention was devoted to analyzing the effect of the thickness of deposited SiC thin films on optical properties.

II. EXPERIMENT

SiC films were deposited on Si (100) substrates at room temperature using an Elettrorava DIBSD system that consisted of a focused Kaufman ion beam source (main ion beam source) and a broad-beam Kaufman ion beam source (assisting ion beam source). The angle between the sputtering beam and the SiC target was fixed at 45° off normal, while the angle between the assisting ion beam and the substrate was maintained at 60°. The assisting ion beam was turned on for 5–10 min for substrate precleaning with low energy Ar ion bombardment. During deposition, the assisting ion beam was turned on to reduce the columnar growth and hence growth uniformity and improved film adhesion to the substrate were achieved.[29] Before the growth process, the Si substrates were cleaned in trichloroethylene, acetone, isopropanol, and de-ionized water and subsequently purged by 5*N*-purity (99.999%) nitrogen gas to remove dust particles. The degreased Si substrates were then immersed in HF solution to remove the native oxide and form a hydrogen-terminated Si surface. Argon gas with 99.999% purity was used as the main source gas for ion beam generation from a high purity 4-in. diameter SiC sputtering target mounted on a rotatable, water-cooled target holder inside the DIBSD chamber. The working pressure of argon was 2.8×10^{-4} mbar. During deposition, the voltage and the current of the main sputtering beam were 800 V and 55 mA, while the discharge voltage and the current of the assisting ion source were kept constant at 60 V and 600 mA, respectively, during all thin film depositions. SiC films of variable thicknesses were deposited at room temperature[9,20,30] by changing the deposition times with a constant radio frequency power of ~70 W fed to the sputter ion beam source. Since it is well known that the thin films deposited with ion beam sputter deposition technology at room temperature undergo only a weak or negligible thermal induced extrinsic stress,[30] in this work, DIBSD at room temperature was employed for the SiC thin film deposition. *Ex situ* annealing of grown SiC films was performed in vacuum ($\sim 1 \times 10^{-3}$ mbar) at 100 °C for 10 h in a high temperature tube furnace (Nabertherm, Germany) system to reduce any possible intrinsic film stress.[30] A set of SiC thin films with varying film thicknesses from ~20 nm to ~450 nm were grown on Si substrates. The representative SiC films of thickness ~20, ~80, ~200, and ~450 nm will be referred as SiC-1, SiC-2, SiC-3, and SiC-4, respectively, hereafter.

The thicknesses of the films, their electron density profiles (EDPs) along the surface normal, and the surface and interface roughness were estimated using XRR measurements. XRR data were collected using a Rigaku SmartLab automated multipurpose x-ray diffractometer with CuK_α radiation ($\lambda = 1.54$ Å) operating at 40 kV and 30 mA. In XRR studies under the specular condition, the scans were performed in the plane containing the incident beam and the surface normal, with an incident angle α_i equal to the scattering angle α_f and α_i varying from 0° to 5.5°. Under this geometrical condition,

the momentum transfer vector, $q = k_f - k_i$ with $k_{f(i)}$ being the scattered (incident) x-ray wave vector, has its only nonvanishing component along the normal to the sample surface, q_z [$=(4\pi/\lambda)\sin\alpha_i$]. The reflectivity data of SiC films were analyzed by Parratt formalism.[31–34] This scheme recursively solves Fresnel equations at each interface, i.e., the change in electron density (ρ) within any film.[31] The extracted values of film thickness, electron density, and interface width or roughness from the best fit of reflectivity data were used to construct the EDPs, i.e., the electron density as a function of film depth from the top for SiC/Si systems, after convoluting the profile with the interface widths.[35–41]

The morphology and the roughness of the SiC films were examined by field emission gun-scanning electron microscopy (Supra 55 Zeiss) and AFM in the tapping mode using a Bruker Dimension 3100 icon with Nanoscope V. The structure of the deposited SiC films was examined by XRD with CuK_α radiation ($\lambda = 1.54$ Å) using a Rigaku SmartLab automated multipurpose x-ray diffractometer. The bonding configuration and compositional information were estimated by FTIR spectroscopy and Raman scattering. For FTIR spectroscopy, a Tensor 27 Bruker spectrometer was employed. Transmission spectra were obtained in the frequency range from 600 to 3500 cm^{-1} with a resolution of 2 cm^{-1}. A Raman spectrometer (LabRAM HR Evolution, Horiba Scientific) with a 633 nm He-Ne laser of 5 mW power focused to a spot of the size of 0.8 μm diameter was used for Raman scattering measurements.

SE measurements of the ellipsometric angles ψ and Δ were performed on SiC thin films deposited on Si substrates with a variable-angle rotating-analyzer ellipsometer equipped with a computer-controlled Berek waveplate compensator (J.A. Woollam, Co., Lincoln, NE, Model: VASE) in the photon energy range of 0.55–6.3 eV at three incident angles of 60°, 65°, and 70°, similar to the technique described elsewhere.[42] Ellipsometry techniques have been extensively used to explore the optical properties of the thin films, namely, complex dielectric function, absorption coefficient, and bandgap along with the film thickness and roughness, using WVASE (J.A. Woollam, Co.) software.

III. RESULTS AND DISCUSSIONS

A. Optical properties of SiC on Si thin films

The optical properties of SiC thin films of different thicknesses (SiC/Si) were analyzed by SE, as shown in Fig. 1. The main advantages of the SE technique are its precision and nondestructiveness and, particularly, the ability to measure the thicknesses and the optical constants of the system simultaneously.[43] In this SE study, to extract the optical constants of the SiC films, a three-layer model (i.e., surface roughness/SiC layer/Si substrate) was employed as shown in Fig. 1(e), where the Si substrate is about 1 mm thick and has been treated as infinite. The optical constants of Si are well known.[44] Surface roughness is described with an effective medium approximation (EMA) layer that is used to simulate the small amount of interfacial intermixing or surface roughness.[45] It is mostly of

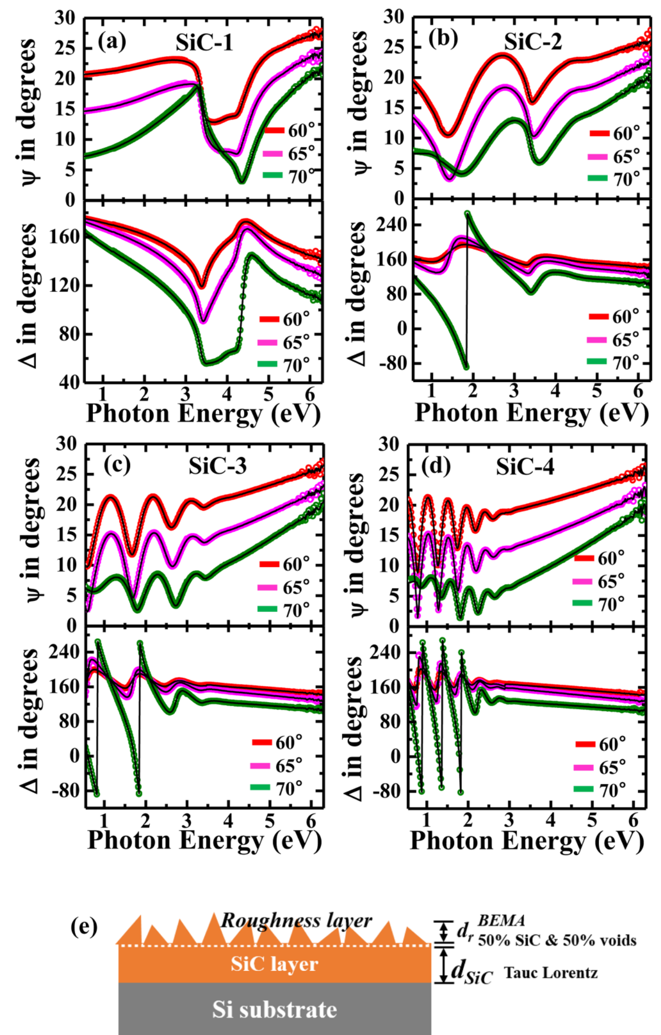

FIG. 1. Ellipsometric angles ψ and Δ vs photon energy for (a) SiC-1, (b) SiC-2, (c) SiC-3, and (d) SiC-4 at angles of incidence 60°, 65°, and 70°. The best fits to the data using a Tauc–Lorentz model with roughness are shown by solid lines. (e) The optical model used to fit the ellipsometric data, consisting of a Si substrate, a SiC film, and a roughness layer.

the same material as the underlying layer with a void fraction of 50%, the combined effect of roughness and porosity.[46] A Tauc–Lorentz (TL) optical function was applied to model the deposited SiC layers on Si. The Tauc–Lorentz expression for the absorption coefficient that is directly related to the imaginary part of the dielectric function is given by[47,48]

$$\varepsilon_2 = \frac{AE_0C(E-E_g)^2}{(E^2-E_0)^2 + C^2E^2}\cdot\frac{1}{E}\ (E > E_g) \qquad (1)$$
$$= 0\ (E \le E_g),$$

$$\varepsilon_1 = \varepsilon_\infty + \frac{2P}{\pi}\oint\frac{\xi\varepsilon_2}{\xi^2 - E^2}d\xi, \qquad (2)$$

where A is the transition matrix element (proportional to the magnitude of the real and imaginary part of complex dielectric constant), E_0 corresponds to peak transition energy, C is the Lorentz broadening term, and E_g corresponds to the optical

bandgap.[47,48] The additional fitting parameter, ε_∞, is the high-frequency dielectric constant, and P stands for the Cauchy principal part of the integral. Figures 1(a)–1(d) show the ellipsometric angles ψ and Δ as a function of photon energy, for SiC-1, SiC-2, SiC-3, and SiC-4, respectively. We found that the calculated ψ and Δ are in good agreement with the experimental data. Excellent fits with mean-squared-error below 10 were achieved for all our samples. It is observed that the optical behavior of the sample has a clear trend that evolves with thickness. The SiC layer thicknesses for SiC-1, SiC-2, SiC-3, and SiC-4 as estimated from the excellent fits of ellipsometry data are 21.6, 81.7, 199, and 447.2 nm, respectively. A 2–4 nm roughness layer above the SiC layer in all the samples was determined.

The dielectric function $\varepsilon(E) = \varepsilon_1(E) + \varepsilon_2(E)$, for SiC thin films, is determined by SE in the 0.55–6.3 eV photon energy range at room temperature using the optical model described above. After obtaining the SiC layer thickness, n and k were also independently varied wavelength-by-wavelength across the entire spectral range to fit the ellipsometric data using the point-by-point method. The calculated ε_1 and ε_2 using the best-fit parameters are shown in Fig. 2. A closer observation of the ε_1, ε_2 spectra in Fig. 2 shows a drop in the real and imaginary parts of a complex dielectric function as the film thickness is increased.

Lines show the optical constants (dielectric function) derived from the TL fit, while the symbols (open circles) show the optical constants derived from point by point fit (point by point_TL).

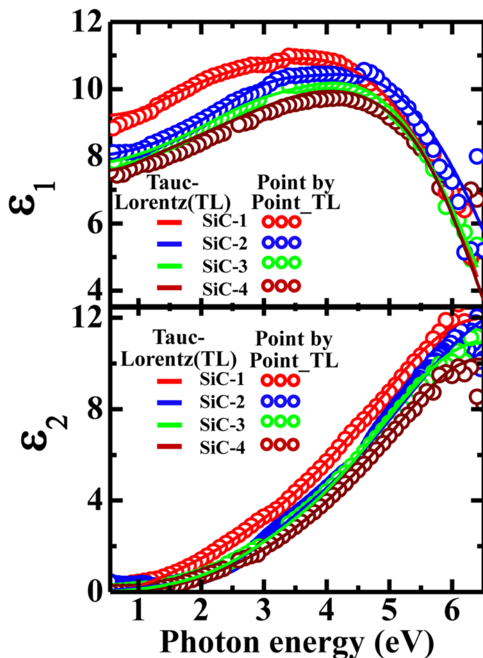

Fig. 2. Spectra for real (ε_1) and imaginary (ε_2) parts of the dielectric function for SiC-1 (~20 nm), SiC-2 (~80 nm), SiC-3 (~200 nm), and SiC-4 (~450 nm) thin films of SiC in the SiC/Si system. These optical constants were determined from a wavelength-by-wavelength fit as described in the text. Lines show the optical constants (dielectric function) derived from TL fit, while the symbols (open circles) show the optical constants derived from point by point fit (point by point_TL).

The refractive index n and the extinction coefficient k were also calculated from the values of ε_1 and ε_2 using the following equation:[49,50]

$$\varepsilon_1 = n^2 - k^2, \quad (3)$$

$$\varepsilon_2 = 2nk. \quad (4)$$

Figure 3(a) shows the evolution of the refractive index n with wavelength for SiC-1, SiC-2, SiC-3, and SiC-4 thin films. It has a broad maximum at about 300 nm and decreases toward longer wavelengths. Extrapolating spectral refractive indices to the nonabsorbing region their values n_∞ in the long wavelength limit[16] at 2140 nm were estimated and included in Table I. The refractive index n_∞ is an important wavelength-independent optical parameter related to the atomic structure and the mass density. Interestingly, we have a decrease in the refractive index with the increase in the thickness of SiC thin films as shown in Fig. 3(b). The change in optical constants (real and imaginary parts of the complex dielectric function and refractive index) with thickness indicates that thickness induces variation in

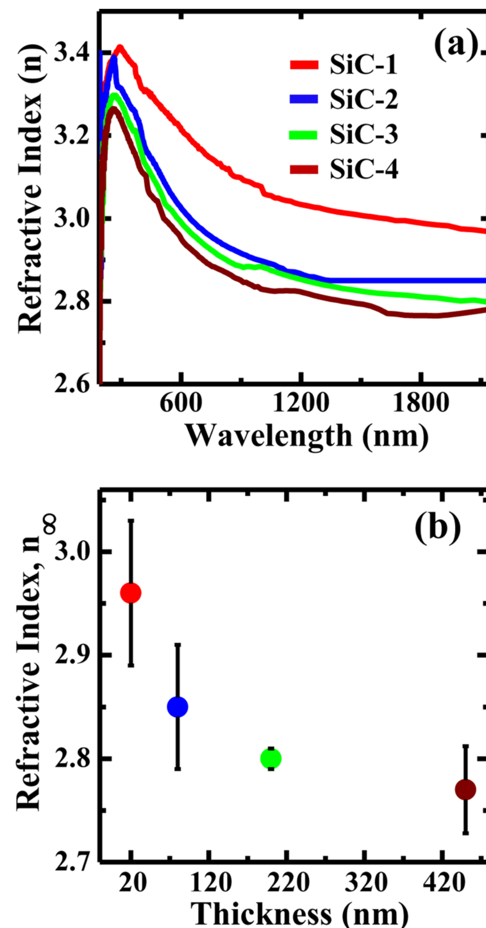

Fig. 3. (a) Refractive index (n) as a function of wavelength for SiC-1 (~20 nm), SiC-2 (~80 nm), SiC-3 (~200 nm), and SiC-4 (~450 nm) thin films of SiC in the SiC/Si system. (b) Variation of high-frequency refractive index, n_∞ with SiC film thickness.

TABLE I. Various parameters extracted for our SiC on Si layers. n_∞ is the long-wavelength refractive index at 2480 nm, E_g is the direct bandgap, p_v is the void fraction from the BEMA, and ρ_{rel} is the electron density (relative to bulk SiC).

	Ellipsometry					XRR					AFM
Sample	Film thickness (nm)	Surface roughness (nm)	n_∞	p_v (%)	Bandgap (eV)	Film thickness (nm)[b]	Average electron density (eÅ^{-3})	Surface roughness (nm)	ρ_{rel} (%)	p_v[a] (%) (from XRR)	Surface roughness (nm)
SiC-1	21.6 ± 0.1	3.2	2.97 ± 0.07	0	5.15 ± 0.07	21.6	0.84	0.5	85.8	14.19	0.6
SiC-2	81.7 ± 0.1	2.9	2.85 ± 0.06	6.05	5.22 ± 0.05	82.5	0.89	0.5	90.9	9.09	0.5
SiC-3	199 ± 0.1	2.4	2.82 ± 0.01	8.51	5.31 ± 0.08	203	0.90	0.4	91.93	8.06	–
SiC-4	447.2 ± 0.1	2.6	2.77 ± 0.04	11.51	5.59 ± 0.07	456	0.92	0.4	93.97	6.02	0.3

[a] $\rho_v = 100 - \rho_{rel}$, where ρ_v is the void fraction.
[b] Experimental resolution in the determination of film thickness from XRR is π/q_{max}, which is ∼0.6 nm for thinner SiC films, SiC-1 (21.6 nm) and SiC-2 (∼82 nm), but for thick films of thicknesses ∼199 nm and ∼447 nm, determination of thickness from XRR is very less sensitive, which involves high error bars[34] [q_{max} can be obtained from Fig. 5(a)].

composition ratio or rearrangement of bonds or changes in the number of defects or defect levels, which may result in a change in the structure of SiC.[46,51,52]

The direct bandgap E_g is estimated from the absorption coefficient α, which was calculated from k, using the values of ε_1 and ε_2.[53] Figure 4(a) displays a Tauc plot[54,55] obtained with the present optical constants by the fitting equation for a direct bandgap semiconductor,

$$\alpha E \propto (E - E_g)^{1/2}.$$

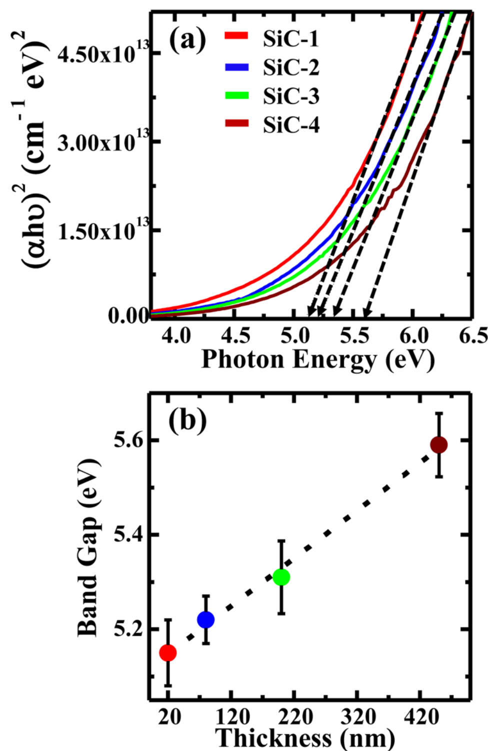

FIG. 4. (a) Plot of $(\alpha h\upsilon)^2$ vs photon energy for SiC-1 (∼20 nm), SiC-2 (∼80 nm), SiC-3 (∼200 nm), and SiC-4 (∼450 nm) thin films of SiC on Si. (b) Direct bandgap variation with SiC film thickness (symbols), where the black dotted line represents exponential growth.

The absorption coefficient as a function of photon energy evidenced a shift of the bandgap toward higher energies from 5.15 to 5.59 eV with increased SiC film thicknesses. The variation of the direct bandgap with thickness is shown in Fig. 4(b). The experimental data (symbols) are fitted with an exponential curve (dotted line). This exponential increase of the direct bandgap with SiC film thickness excludes quantum confinement in a thinner film as an explanation.

It is noteworthy to mention that the observed range of direct bandgap (5.15–5.59 eV)[56–58] and refractive index (2.77–2.97)[52,59] of the SiC films (SiC-1, SiC-2, SiC-3, and SiC-4) are in accordance with the results reported by other research groups.

It should be noted that a refined analysis was also employed, using a graded layer model (simple graded index model or graded layer model), to fit the SE data[60–63] for SiC films and to confirm the findings on thickness dependent variation in optical constants for DIBSD grown SiC films, and the same has been discussed in detail in S1 in the supplementary material.[113]

The tunable optical properties of the SiC films cannot be explained by the well-known quantum confinement effect[64] as the results indicate the opposite trend. The known increase (decrease) of the refractive index when the optical bandgap decreases (increases) is an indication of a material structure change,[65] which can be attributed to different factors. Film density is one of the controlling factors for the variation of material structures and consequently the refractive index of SiC films. The film density change may be caused by voids present in the material similarly as reported by Webman *et al.*[66] The refractive index of our amorphous SiC films can be related to the refractive index of a reference material (taken to be the thinnest film SiC-1) and air ($n_{void} = 1$) using Bruggeman effective medium approximation (BEMA) models,[67] as described in S2 in the supplementary material.[113] So, there is a possibility that the observed decrease in refractive index with an increase in the thickness of SiC films could be an effect of the increase in the void density of the SiC films. X-ray reflectivity has been employed to explore and verify the possibility of enhancement of the void density in the SiC thin films with decreasing film thickness, as discussed in Sec. III B.

Secondly, different polytype crystal structures (3C-SiC, 6H SiC, etc.) have different electronic and optical properties.[68,69]

Also, the optical properties depend on the crystallinity (amorphous/polycrystalline) state of the SiC system.[69] In this context, the crystal structures of the SiC films were investigated by XRD to explore the reason behind the observed thickness dependent changes in the optical properties in SiC, as described in Sec. III C.

Furthermore, it is also known that the optoelectronic properties of silicon carbon alloys are dependent on the carbon content.[70,71] The ratio of carbon to silicon has been known to be responsible for varying optical properties, specifically the change in refractive index and bandgap, of the SiC structure as demonstrated by other research groups.[59,72,73] In view of these, the ratio of compositional content and bonding configuration of the SiC thin films were analyzed and discussed in Secs. III D and III E to explain the observed trend in the optical properties of SiC films of different thicknesses.

B. Electron density profile of SiC thin film through XRR

As discussed above the change in the refractive index can be attributed to the change in the density of the SiC film. This film density change may be caused by voids present in the material.[16,67] The electron density that is proportional to mass density (film density) is used to estimate the void density in the grown SiC thin films. Electron density profiles normal to the surface of SiC films were studied using specular x-ray reflectivity (XRR) through which thickness, surface, and interface roughness were also estimated.

For characterization of single/multilayer thin film systems of nanometer-scale surface/interface roughness of any kind of materials, XRR[74–76] is an ideally suited nondestructive technique to probe the buried interfaces to determine the layers' thickness, surface/interface roughness, and electron density profile, without suffering from charging effects, and providing excellent depth sensitivity.[77] Moreover, for XRR, any special sample preparation technique/sputtering [such as for cross-sectional TEM and SEM (Refs. 78 and 79)] is not a prerequisite.[78,80–84] XRR provides a statistical averaging over the whole sample area, since it involves probing a surface at microscopic length scales while sampling a macroscopic portion of the surface[85] thus sampling in the same way as in macroscopic characterization techniques.[77]

In specular x-ray reflectivity, incident angle (α_i) and scattering angle (α_f) are equal to each other, as shown schematically in Fig. 5. The surface normal component of the wave vector transfer is q_z, where $q_z = (4\pi/\lambda)\sin\alpha_i$. The x-ray reflectivity, $R(q_z)$, is related to the electron density $\rho(z)$ via the following expression:[34,37,86]

$$R(q_z) = R_F(q_z)\left|\frac{1}{\Delta\rho_z}\int\frac{d\rho(z)}{dz}\exp\left(-iz\sqrt{q_z(q_z^2-q_c^2)^{\frac{1}{2}}}\right)dz\right|^2, \quad (5)$$

where R_F is the Fresnel reflectivity from a single ideal interface, $\Delta\rho_z$ is the total change in electron density across the interface (along surface normal), and q_c is the momentum

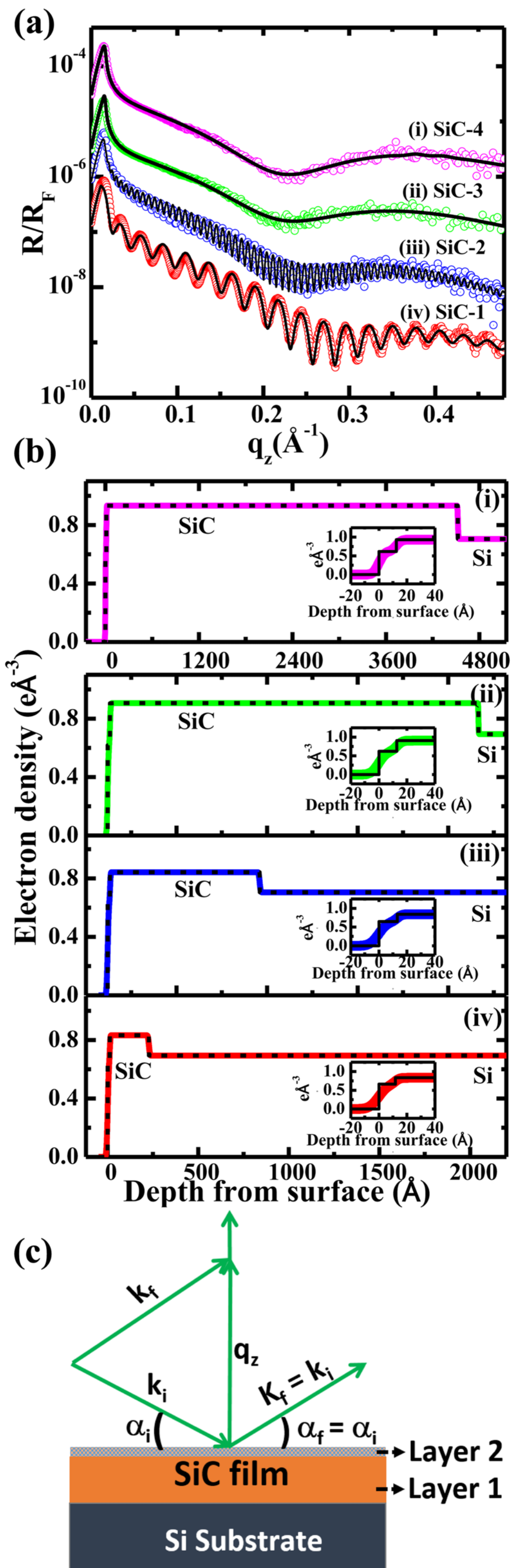

FIG. 5. (a) Fresnel normalized x-ray reflectivity (R/R_F) for (i) SiC-1, (ii) SiC-2, (iii) SiC-3, and (iv) SiC-4; circles and lines represent experimental data and theoretical fit, respectively. (b) Corresponding EDPs of SiC/Si thin films. Inset of (b) shows the zoomed portion of the EDP of SiC, which indicates the presence of a very thin layer (∼1 nm) of SiC with slightly lower electron density, above the thick primary SiC layer. (c) Schematic representation of specular x-ray reflectivity (XRR) for SiC/Si layers: α_i and α_f denote the incident and scattered angles of x-ray, respectively, and q_z is the momentum transfer vector component perpendicular to the sample surface.

transfer at the critical angle for total external reflection. Equation (1) was used to extract the electron density profile by analyzing the XRR data of SiC/Si using Parratt formalism.[31,41]

Figure 5(a) shows Fresnel normalized x-ray reflectivity (R/R_F)[32,41] data of films with different SiC thicknesses, namely, SiC-1, SiC-2, SiC-3, and SiC-4, where circles and lines represent experimental data and theoretical fit, respectively. Interference of scattered x-rays from SiC/Si layers results in the formation of a pattern of well-defined Kiessig fringes of films with finite thickness as shown in the reflectivity pattern of the films in Fig. 5(a). A secondary pattern of Kiessig fringes is evident in XRR pattern with a larger period of oscillations, corresponding to a large change in q_z, indicating the presence of a thin layer of different electron density along with the thicker layer in SiC/Si systems. The x-ray reflectivity data have been fitted by the well-known Parratt exact recursive method.[31] Initially, a single layer model on top of the substrate is tested. A reasonable agreement between theoretical fit and experimental data is not obtained as the secondary pattern in the XRR is not properly represented by this single layer model. An improvement of the data fitting is obtained by the introduction of a very thin layer on the top of the main SiC layer. The EDP along the surface normal direction has been extracted by fitting the XRR data with the above theoretical model using Parratt formalism by recursively solving the Fresnel equations at each interface,[31] shown in Fig. 5(b). A schematic of the XRR technique for SiC/Si layers is depicted in Fig. 5(c). Electron density profiles indicate the formation of SiC films on a Si substrate, with very low surface and interface roughness (<5 Å). It is to be noted that the extracted EDP indicates the presence of a very thin layer (~1 nm) of SiC with slightly lower electron density (0.664 e$Å^{-3}$), above the thick principal SiC layer in all the SiC/Si films as shown in the zoomed portion of EDP in the inset of Fig. 5(b). The result is consistent with the observed overall surface roughness of SiC/Si films as obtained from SE data analysis. The overall thicknesses of SiC layers as estimated from XRR are 21.6, 82.5, 203, and 456 nm for SiC-1, SiC-2, SiC-3, and SiC-4, respectively. The thicknesses of SiC films, as determined from the XRR, are in good agreement with the results obtained from the SE study, as shown in Table I. The electron densities of SiC films are very close to the bulk SiC electron density (ρ_{bulk} = 0.979 e$Å^{-3}$) and found to vary only slightly with the thickness of the SiC thin films (see Table I). The XRR analysis shows the formation of high-quality SiC thin films, with nearly full coverage (>90%, as calculated from the bulk electron density of SiC) and very low surface roughness (see Table I).

The relative electron density (ρ_{rel}) of each film with respect to the SiC bulk electron density (ρ_{bulk} = 0.979 e$Å^{-3}$) is shown in Table I. The results indicate a small increase in electron density in thicker SiC films (by less than 10%), consequently a decrease in void density in thicker films. Therefore, the observed increase of refractive index in thinner SiC film cannot be explained by the influence of void density in the SiC film, because opposite trends are observed in SE and XRR as a function of SiC layer thickness.

C. Structural analysis by XRD

The influence of crystallinity on the observed changes in optical properties of the deposited SiC thin films of different thicknesses was also investigated. Different crystal structures (amorphous or crystalline) of SiC are known to have different optical properties as reported in the literature.[68,69] XRD patterns of SiC films (SiC-1, SiC-2, SiC-3, and SiC-4) show that the films are amorphous in nature, as shown in Fig. S3 in the supplementary material.[113] The XRD patterns exhibit a peak at 2θ of 69°, which corresponds to the (004) Si substrate Bragg peak, but there is no diffraction peak of crystalline SiC, indicating that the films can be regarded as amorphous SiC.[72]

The thickness independent amorphous nature of DIBSD deposited SiC films rules out the influence of crystal structure to explain the observed variation of optical properties of SiC films.

D. Bonding configuration/compositional study by FTIR and Raman spectroscopy

The SiC films were analyzed by FTIR and Raman spectroscopy in order to investigate the bonding configuration and compositional details. Figure 6 shows the FTIR transmittance spectra of SiC/Si layers (SiC-1, SiC-2, SiC-3, and SiC-4) in the region of 500–3500 cm^{-1}. The FTIR spectrum of the Si substrate is also shown as a reference. Several FTIR absorption bands were detected from the SiC/Si layers including the Si–C stretching vibration[87,88] at 820 cm^{-1}, the Si-H oscillatory modes[65] at 885 cm^{-1}, and the C-H wagging mode[87] at 970 cm^{-1}. Absorption at 1200–1000 cm^{-1} corresponds to Si–O–Si and Si–O–C bonds.[65] The peak at position ~740 cm^{-1} in the Si substrate can be assigned to the two-phonon modes (LO + LA) of Si (Ref. 89), while the peak at a similar position for SiC films, which becomes stronger for thicker SiC films, may have an additional contribution from the C–C bonds.[9] The spectrum of the thickest (SiC-4) SiC film shows a broad absorption band between 630 and 1050 cm^{-1}, which can be deconvoluted into C–C, Si–C, Si–H, and C–H bonds, as shown in Fig. 6. The broad

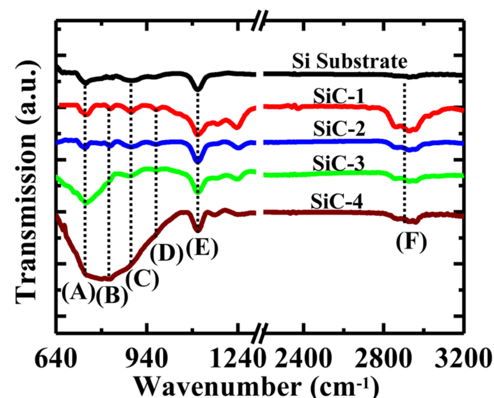

Fig. 6. FTIR spectra of different SiC/Si thin films. (A) two-phonon modes (LO + LA) modes of Si and/or C–C bond; (B) Si–C bond; (C) Si–H oscillatory mode; (D) C–H wagging mode; (E) Si–O–Si and Si–O–C bonds; (F) C–H stretching vibration.

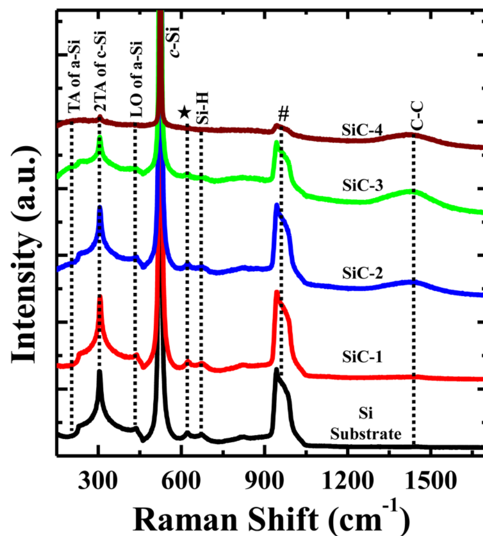

Fig. 7. Raman spectra of different SiC/Si thin films with respect to the Si substrate. *c*-Si represents the crystalline Si substrate.

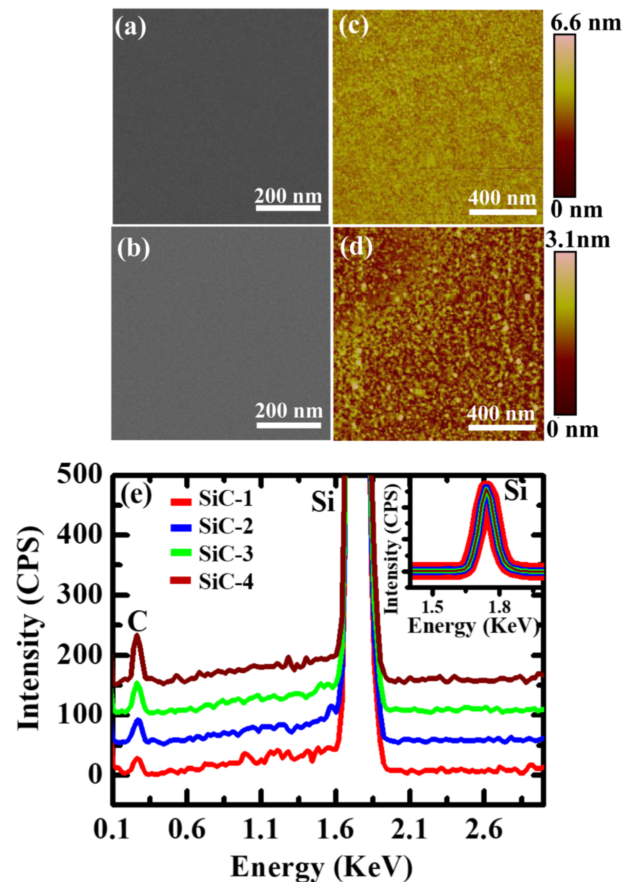

Fig. 8. FESEM image of SiC/Si thin film (a) SiC-4 and (b) SiC-1. Corresponding tapping mode AFM topographic images [(c) and (d)]. (e) Carbon signal relative to Si, using EDAX spectra of SiC films of different thicknesses. Inset: normalized Si signal.

absorption band is indicative of the amorphous structure of the grown SiC films,[88,90] as revealed by XRD also. An absorption band at around 1100 cm^{-1}, assigned by Si–O–Si or Si–O–C bonds,[91,92] could be induced by the Si substrate. Additionally, an absorption band in the range of 2800–3000 cm^{-1} is detected in all the SiC/Si layers, which is attributed to the C-H stretching vibration.[93]

Figure 7 shows the Raman spectra of SiC/Si systems (SiC-1, SiC-2, SiC-3, and SiC-4). Raman scattering was employed to the SiC/Si layers as a complementary technique to FTIR spectroscopy. A sharp peak at 520 cm^{-1} and a broad band near 970 cm^{-1} correspond to the TO and two-phonon 2TO of the crystalline Si substrate.[94–96] The peak at ∼300 cm^{-1} can be assigned to the second transverse acoustic phonon mode (2TA) of the Si substrate.[96] The weak peak at 620 cm^{-1} can be assigned as an overtone of the peak at about 300 cm^{-1}, originating from the crystalline bulk Si substrate,[97,98] while the peak at 670 cm^{-1} can be attributed to the wagging vibrations of Si–H bonds.[99] For the thicker SiC films (SiC-2, SiC-3, and SiC-4), a broad band appearing in the 1300–1500 cm^{-1} spectra region is associated with the C–C vibrational modes.[100] This C–C signature was already observed in Si–C alloys with carbon excess certainly corresponding to a specific structure, which could be described as a random covalent network of tetrahedral–trigonal bonding carbons with distorted bond angles and bond length.[94,101] The Si–C band, which is usually present in the region of 700 and 1000 cm^{-1}, is found to be very weak in the Raman spectra, which is due to the low Raman efficiency for the Si–C bond because the cross section of the Si–C bond is low as compared to Si–Si and C–C bonds.[73,102] The results indicate the enhancement of C–C bonds in thicker SiC films.

E. Surface morphology and elemental composition ratio

The surface morphology of the SiC/Si thin film was examined by field emission scanning electron microscopy (FESEM) and AFM. Figures 8(a) and 8(b) show the SEM micrograph of SiC-4 and SiC-1, respectively. Corresponding AFM images are displayed in Figs. 8(c) and 8(d). Images show the smooth and uniform surface morphology for both the SiC films. Root mean square roughness of the obtained film estimated from a 5 $\mu m \times 5 \mu m^2$ AFM scan are given in Table I. The roughness was found to be very low (<5 Å), which is consistent with the surface roughness obtained from XRR that signifies the deposition of the smooth SiC film. It is to be noted that similar smooth films with no grain formation are observed in all the thicknesses of SiC deposited, which rules out the possibility that different particle morphology and size influence the observed changes in optical properties.

It is well known that in amorphous SiC alloys, the optical gap and the refractive index strongly depend on film composition.[103,104] This change in carbon content has been related to changes in the optical properties of SiC by many research groups.[9,12,59,72,73] They had demonstrated that with increasing C content with respect to Si, there was an increase in bandgap and a decrease in refractive index in SiC.[73,105] In that respect, EDAX measurement was carried out to explore the compositional information[106–108] of the SiC/Si layers of different thicknesses in our study. Figure 8(e) represents EDAX spectra of SiC films. A clear indication of enhancement of the C signal in thicker SiC films was observed in EDAX

spectra of those with normalized Si signal, as shown in Fig. 8(e) and the inset.

The increasing carbon (C) to silicon (Si) atomic concentration ratio (C:Si) with increasing SiC film thickness is evident from EDAX results. The enhancement of C:Si ratio from about 0.6 to 1.1 concomitant to the increase in the SiC film thickness from 20 nm (SiC-1, the thinnest SiC film) to 450 nm (SiC-4, the thickest SiC film). It should be noted that for these SiC films, the C:Si ratio reaches the saturation value, which is close to 1.1, when SiC film thickness reaches about 400 nm, and remains the same for the 450 nm thick SiC film, as shown in S4 and Fig. S4 in the supplementary material[113] (and consequently in S5 and Fig. S5 in the supplementary material[113]). The observed enhancement in the carbon content in a thicker SiC film can be attributed to the decrease in the refractive index and an increase in the bandgap. In that respect, the observed thickness dependent variation in the refractive index and the bandgap of the SiC thin film can be properly explained/correlated in terms of variation of the C:Si ratio.

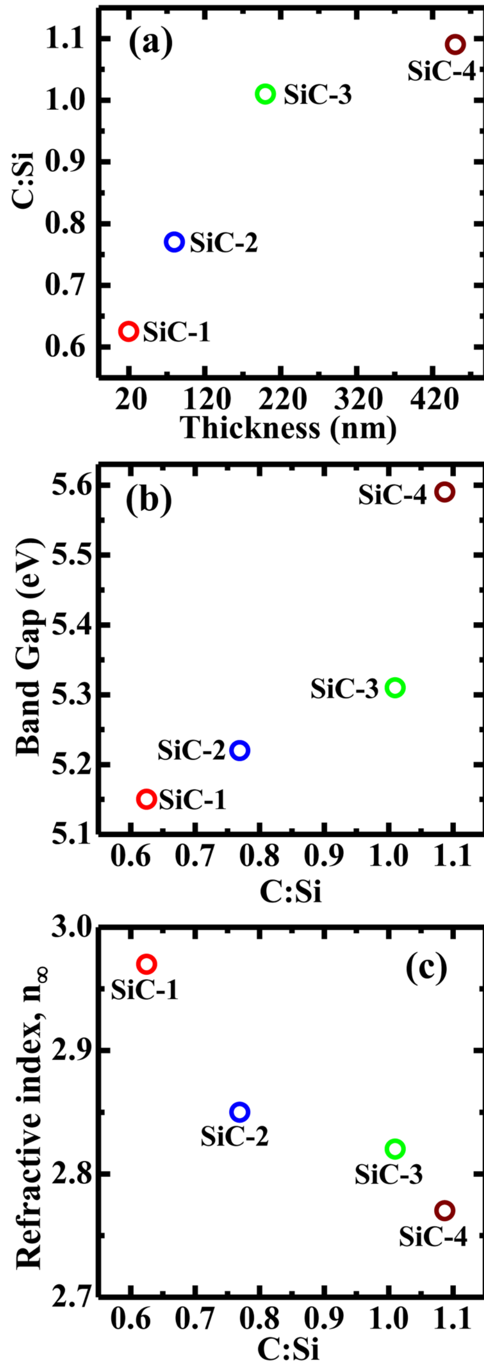

FIG. 9. (a) Increment of C:Si with SiC film thickness. Variation of bandgap (b) and refractive index n_∞ (c) with the C to Si ratio (C:Si) in SiC films of different thickness.

The variation of the ratio of C:Si with thickness is represented graphically in Fig. 9(a). The variations of bandgap and high-frequency refractive index (n_∞) with the increment of C:Si ratio are shown in Figs. 9(b) and 9(c), respectively.

The observed increase in the Tauc bandgap with thickness in this study is found to be in parallel with the increment in the carbon content as reported earlier.[109–111] This can be attributed to the structural change of the films from Si-rich thinner *a*-SiC films to near stoichiometric (Si:C = 1:1) thicker *a*-SiC films as the replacement of weaker Si–Si bonds in Si-rich films with stronger Si–C bonds in thicker SiC influences the energy band structure through the lowering of the valence band edge.[73,105] The reduction in the contents of C would cause a reduction in the chemical shift of the valence band states to higher energy and, therefore, would result in a decrease in the E_g values. These results suggest that the key parameter controlling the energy bandgap is being regulated by the C:Si atomic ratio. The refractive index of the SiC/Si layer shows the decrease in the refractive index (n_∞) with an increase in thickness, which can also be attributed to the increase in the carbon content.[73,105,112]

IV. CONCLUSIONS

Amorphous SiC thin films with high coverage and low surface/interface roughness were prepared by the DIBSD technique on Si substrates. Film thicknesses of SiC layers were varied from about 20 to 450 nm. Thickness dependent optical properties of SiC thin films were explored by SE. Interestingly, the refractive index of SiC thin films was found to be decreasing from 2.97 to 2.77 with increasing film thickness from 20 to 450 nm, whereas the bandgap was increasing from 5.15 to 5.59 eV with increasing SiC film thickness in the same range. The observed thickness dependent variation in optical properties was suitably explained by the increment of C to Si atomic concentration ratio in SiC thin film with increasing film thickness from 20 to 450 nm, as extracted from EDAX measurement. The other possible explanations, such as the increase of void concentration in the thicker SiC films or change in crystallite size/crystallinity/formation of a different crystalline polytype of SiC in the thicker films, were excluded by using relevant measurements (e.g., XRR, XRD, Raman spectroscopy, SEM, and AFM). The study has established a control of optical properties of amorphous SiC thin films corresponding to its structural properties or composition ratio by way of changing the film thickness and has important implications in terms of various diverse applications of SiC thin films, such as solar cell,

optoelectronic devices (e.g., photoreceptors and color sensors), and photovoltaic applications. The unique properties of amorphous SiC have already made it a suitable candidate for solar cells and photovoltaic applications in its thin film form. The results developed in this study can be used for further optimizing the performance of SiC in various applications through tuning of optical properties.

ACKNOWLEDGMENTS

The authors would like to acknowledge IIT Indore for all kinds of support to this work and the Sophisticated Instrument Centre (SIC) at IIT Indore for DIBSD, FESEM, EDAX, and FTIR facilities. They would also like to acknowledge Project No. SR/FST/PSI/225/2016 under FIST program of DST, Government of India, for the Raman characterization facility. The work at NMSU was supported by the National Science Foundation (No. DMR-1505172). This work is partially supported by the Council of Scientific and Industrial Research (CSIR), India, Project No. 03 (1310)/14/EMR-II, and the Department of Science and Technology (DST), India, Project No. SB/S2/CMP-077/2013.

[1]J. Casady and R. W. Johnson, Solid·State Electron. **39**, 1409 (1996).
[2]A. Höfgen, V. Heera, F. Eichhorn, and W. Skorupa, J. Appl. Phys. **84**, 4769 (1998).
[3]A. Ávila, I. Montero, L. Galan, J. M. Ripalda, and R. Levy, J. Appl. Phys. **89**, 212 (2001).
[4]W. Lambrecht, B. Segall, W. Suttrop, M. Yoganathan, R. Devaty, W. Choyke, J. Edmond, J. Powell, and M. Alouani, Appl. Phys. Lett. **63**, 2747 (1993).
[5]E. J. P. Santos, R. P. Ribas, J. W. Swart, E. S. E. Division, S. B. d. Microeletrônica, and S. B. d. C. C. Ao, *Microelectronics Technology and Devices, SBMICRO 2004 Proceedings of the Nineteenth International Symposium*, Porto de Galinhas, Pernambuco State, 4–11 September 2004 (Electrochemical Society, Pennington, NJ, 2004).
[6]D. Massoubre, L. Wang, J. Chai, G. Walker, L. Hold, M. Lobino, S. Dimitriev, and A. Iacopi, NSTI-Nanotech **2**, 416 (2014).
[7]Y.-H. Joung, H. I. Kang, J. H. Kim, H.-S. Lee, J. Lee, and W. S. Choi, Nanoscale Res. Lett. **7**, 22 (2012).
[8]S. Janz, S. Reber, and S. Glunz, *Proceedings of the 21st EUPVSEC*, Dresden, Germany, 4–8 September 2006 (WIP-Renewable Energies, München, Germany 2006), p. 660.
[9]C. Jin, T. Yu, Y. Zhao, Y. Bo, X. Wu, and L. Zhuge, Physica E **43**, 1863 (2011).
[10]T. Chen, Y. Huang, A. Dasgupta, M. Luysberg, L. Houben, D. Yang, R. Carius, and F. Finger, Sol. Energy Mater. Sol. Cells **98**, 370 (2012).
[11]M.-H. Kao, C.-H. Shen, P.-C. Yu, W.-H. Huang, Y.-L. Chueh, and J.-M. Shieh, Sci. Rep. **7**, 12706 (2017).
[12]T. Ma, J. Xu, K. Chen, J. Du, W. Li, and X. Huang, Appl. Phys. Lett. **72**, 13 (1998).
[13]A. Koji, T. Akio, O. Akifumi, and O. Hisahito, Jpn. J. Appl. Phys. **32**, 590 (1993).
[14]Y. Hamakawa, *Physics and Applications of Amorphous Silicon Carbide* (Springer, Berlin, 1989), p. 164.
[15]B. P. Swain, Surf. Coat. Technol. **201**, 1589 (2006).
[16]J. Müllerová, L. Prušáková, M. Netrvalová, V. Vavruňková, and P. Šutta, Appl. Surf. Sci. **256**, 5667 (2010).
[17]C. C. Liu, C. Lee, K. L. Cheng, H. C. Cheng, and T. R. Yew, Appl. Phys. Lett. **66**, 168 (1995).
[18]Y. Sun, T. Miyasato, J. K. Wigmore, N. Sonoda, and Y. Watari, J. Appl. Phys. **82**, 2334 (1997).
[19]M. Balooch, R. J. Tench, W. J. Siekhaus, M. J. Allen, A. L. Connor, and D. R. Olander, Appl. Phys. Lett. **57**, 1540 (1990).
[20]C. Jin, X. Wu, and L. Zhuge, Adv. Phys. Chem. **2008**, 1 (2008).
[21]B. S. Sengar, V. Garg, V. Awasthi, Aaryashree, S. Kumar, C. Mukherjee, M. Gupta, and S. Mukherjee, Sol. Energy **139**, 1 (2016).
[22]V. Awasthi, S. K. Pandey, S. K. Pandey, S. Verma, M. Gupta, and S. Mukherjee, J. Mater. Sci. Mater. Electron. **25**, 3069 (2014).
[23]S. K. Pandey, S. K. Pandey, V. Awasthi, M. Gupta, U. P. Deshpande, and S. Mukherjee, Appl. Phys. Lett. **103**, 072109 (2013).
[24]A. Kumar, M. Das, V. Garg, B. S. Sengar, M. T. Htay, S. Kumar, A. Kranti, and S. Mukherjee, Appl. Phys. Lett. **110**, 253509 (2017).
[25]A. Kumar, M. Das, and S. Mukherjee, in *Reference Module in Materials Science and Materials Engineering*, edited by S. Hashmi (Elsevier, Oxford, 2018), p. 1.
[26]C. Bundesmann and H. Neumann, J. Appl. Phys. **124**, 231102 (2018).
[27]M. Mateev, T. Lautenschläger, D. Spemann, A. Finzel, J. W. Gerlach, F. Frost, and C. Bundesmann, Eur. Phys. J. B **91**, 45 (2018).
[28]K. Wasa, *Handbook of Sputter Deposition Technology: Fundamentals and Applications for Functional Thin Films, Nano-Materials and MEMS* (Elsevier Science, Waltham 2012).
[29]S. K. Pandey, S. K. Pandey, V. Awasthi, A. Kumar, U. P. Deshpande, M. Gupta, and S. Mukherjee, J. Appl. Phys. **114**, 163107 (2013).
[30]A. Ullah, H. Wilke, I. Memon, Y. Shen, D. T. Nguyen, C. Woidt, and H. Hillmer, J. Micromech. Microeng. **25**, 055019 (2015).
[31]L. G. Parratt, Phys. Rev. **95**, 359 (1954).
[32]S. Chattopadhyay and A. Datta, Phys. Rev. B **72**, 155418 (2005).
[33]S. Chattopadhyay, A. Uysal, B. Stripe, G. Evmenenko, S. Ehrlich, E. A. Karapetrova, and P. Dutta, Phys. Rev. Lett. **103**, 175701 (2009).
[34]S. Chattopadhyay, A. Uysal, B. Stripe, Y.-G. Ha, T. J. Marks, E. A. Karapetrova, and P. Dutta, Phys. Rev. Lett. **105**, 037803 (2010).
[35]J. Als-Nielsen and D. McMorrow, *Elements of Modern X-ray Physics* (Wiley, New York, 2011).
[36]J. Basu and M. K. Sanyal, Phys. Rep. **363**, 1 (2002).
[37]A. Uysal, M. Chu, B. Stripe, A. Timalsina, S. Chattopadhyay, C. M. Schlepütz, T. J. Marks, and P. Dutta, Phys. Rev. B **88**, 035431 (2013).
[38]P. A. Fenter, Rev. Mineral. Geochem. **49**, 149 (2002).
[39]J. Als-Nielsen, D. Jacquemain, K. Kjaer, F. Leveiller, M. Lahav, and L. Leiserowitz, Phys. Rep. **246**, 251 (1994).
[40]A. Singh, S. Schipmann, A. Mathur, D. Pal, A. Sengupta, U. Klemradt, and S. Chattopadhyay, Appl. Surf. Sci. **414**, 114 (2017).
[41]D. Pal, A. Mathur, A. Singh, J. Singhal, A. Sengupta, S. Dutta, S. Zollner, and S. Chattopadhyay, J. Vac. Sci. Technol. A **35**, 01B108 (2017).
[42]C. V. Weiss, J. Zhang, M. Spies, L. S. Abdallah, S. Zollner, M. W. Cole, and S. P. Alpay, J. Appl. Phys. **111**, 054108 (2012).
[43]Q. H. Li, D. Zhu, W. Liu, Y. Liu, and X. C. Ma, Appl. Surf. Sci. **254**, 2922 (2008).
[44]C. M. Herzinger, B. Johs, W. A. McGahan, J. A. Woollam, and W. Paulson, J. Appl. Phys. **83**, 3323 (1998).
[45]Guide to Using WVASE32 by J.A. Woollam Co., Inc.
[46]E. Pascual, J. Andújar, J. Fernández, and E. Bertran, Diamond Relat. Mater. **4**, 702 (1995).
[47]G. E. Jellison and F. A. Modine, Appl. Phys. Lett. **69**, 2137 (1996).
[48]G. JellisonJr., and F. Modine, Appl. Phys. Lett. **69**, 371 (1996).
[49]R. K. Gupta, M. Cavas, and F. Yakuphanoglu, Spectrochim. Acta A Mol. Biomol. Spectrosc. **95**, 107 (2012).
[50]T. S. Moss, G. J. Burrell, and B. Ellis, *Semiconductor Opto-Electronics* (Butterworth, Washington, DC, 2013).
[51]J. K. Saha, B. Bahardoust, K. Leong, A. B. Gougam, N. P. Kherani, and S. Zukotynski, Thin Solid Films **519**, 2863 (2011).
[52]P. Musumeci, R. Reitano, L. Calcagno, F. Roccaforte, A. Makhtari, and M. G. Grimaldi, Philos. Mag. B **76**, 323 (1997).
[53]H. Yoshikawa and S. Adachi, Jpn. J. Appl. Phys. **36**, 6237 (1997).
[54]J. Tauc, *Amorphous and Liquid Semiconductors* (Springer, New York, 2012).
[55]J. Tauc and A. Menth, J. Non-Cryst. Solids **8-10**, 569 (1972).
[56]C. Persson and U. Lindefelt, J. Appl. Phys. **82**, 5496 (1997).
[57]R. Dalven, J. Phys. Chem. Solids **26**, 439 (1965).
[58]J. Fan and P. K. Chu, *Silicon Carbide Nanostructures* (Springer, New York, 2014), p. 7.
[59]P. P. Dey and A. Khare, Mater. Res. Bull. **84**, 105 (2016).
[60]C. L. Bungay, T. E. Tiwald, M. J. Devries, B. J. Dworak, and J. A. Woollam, Polym. Eng. Sci. **40**, 300 (2000).
[61]I. Aulika, S. Corkovic, A. Bencan, S. D'Astorg, A. Dejneka, Q. Zhang, M. Kosec, and V. Zauls, J. Electrochem. Soc. **156**, G217 (2009).
[62]I. Aulika, A. Dejneka, V. Zauls, and K. Kundzins, J. Electrochem. Soc. **155**, G209 (2008).

[63]WVASE Software User Manual, see http://www.jawoollam.com/.
[64]S. Öğüt, J. R. Chelikowsky, and S. G. Louie, Phys. Rev. Lett. **79**, 1770 (1997).
[65]A. Brighet, K. Mokkadem, A. Fedala, and M. Kechouane, Phys. Status Solidi C **7**, 561 (2010).
[66]I. Webman, J. Jortner, and M. H. Cohen, Phys. Rev. B **15**, 5712 (1977).
[67]J. Müllerová, P. Šutta, G. Van Elzakker, M. Zeman, and M. Mikula, Appl. Surf. Sci. **254**, 3690 (2008).
[68]R. P. Devaty and W. J. Choyke, Phys. Status Solidi A **162**, 5 (1997).
[69]M. Kildemo, Thin Solid Films **455-456**, 187 (2004).
[70]M. Kamble *et al.*, Journal of Coatings **2014**, 905903 (2014).
[71]T. Rajagopalan, X. Wang, B. Lahlouh, C. Ramkumar, P. Dutta, and S. Gangopadhyay, J. Appl. Phys. **94**, 5252 (2003).
[72]Y. Cheng, X. Huang, Z. Du, and J. Xiao, Opt. Mater. **73**, 723 (2017).
[73]F. S. Tehrani, B. T. Goh, M. R. Muhamad, and S. A. Rahman, J. Mater. Sci. Mater. Electron. **24**, 1361 (2013).
[74]A. Gibaud, *X-Ray and Neutron Reflectivity: Principles and Applications* (Springer, New York, 1999), p. 87.
[75]E. Chason and T. Mayer, Critical Rev. Solid State Mater. Sci. **22**, 1 (1997).
[76]A. Gibaud and S. Hazra, Curr. Sci. **78**, 1467 (2000).
[77]G. Renaud, R. Lazzari, and F. Leroy, Surf. Sci. Rep. **64**, 255 (2009).
[78]J. Li, T. Malis, and S. Dionne, Mater. Charact. **57**, 64 (2006).
[79]Y. Ding and D. O. Northwood, Mater. Charact. **29**, 25 (1992).
[80]S. Matsui and Y. Ochiai, Nanotechnology **7**, 247 (1996).
[81]P. Russell and F. Stevie, Microsc. Microanal. **8**, 558 (2002).
[82]R. Spolenak, L. Sauter, and C. Eberl, Scr. Mater. **53**, 1291 (2005).
[83]J. Melngailis, Nucl. Instrum. Methods Phys. Res. B Beam Interact. Mater. Atoms **80**, 1271 (1993).
[84]S. Kim, M. J. Park, N. P. Balsara, G. Liu, and A. M. Minor, Ultramicroscopy **111**, 191 (2011).
[85]C. Thompson, G. Palasantzas, Y. Feng, S. Sinha, and J. Krim, Phys. Rev. B **49**, 4902 (1994).
[86]S. Sinha, E. Sirota, S. Garoff, and H. Stanley, Phys. Rev. B **38**, 2297 (1988).
[87]M. Künle, T. Kaltenbach, P. Löper, A. Hartel, S. Janz, O. Eibl, and K.-G. Nickel, Thin Solid Films **519**, 151 (2010).
[88]A. Nazarov, Y. N. Vovk, V. Lysenko, V. Turchanikov, V. Scryshevskii, and S. Ashok, J. Appl. Phys. **89**, 4422 (2001).
[89]P. Olivier and C. Jean-Marc, J. Phys. D Appl. Phys. **45**, 495101 (2012).
[90]J. P. Rivière, M. Zaytouni, M. F. Denanot, and J. Allain, Mater. Sci. Eng. B **29**, 105 (1995).
[91]J. Kim, P. Seidler, L. S. Wan, and C. Fill, J. Colloid Interface Sci. **329**, 114 (2009).
[92]A. Pandey, S. Dutta, R. Prakash, S. Dalal, R. Raman, A. K. Kapoor, and D. Kaur, Mater. Sci. Semicond. Process. **52**, 16 (2016).
[93]L. Wang, J. Xu, T. Ma, W. Li, X. Huang, and K. Chen, J. Alloys Compd. **290**, 273 (1999).
[94]Y. Inoue, S. Nakashima, A. Mitsuishi, S. Tabata, and S. Tsuboi, Solid State Commun. **48**, 1071 (1983).
[95]F. S. Tehrani, Bull. Mater. Sci. **38**, 1333 (2015).
[96]E. Quiroga-González, J. Carstensen, C. Glynn, C. O'Dwyer, and H. Föll, Phys. Chem. Chem. Phys. **16**, 255 (2014).
[97]C. O'Dwyer, *Processes at the Semiconductor-Solution Interface 4* (Electrochemical Society, Pennington, NJ, 2011).
[98]S.-L. Zhang, Y. Hou, K.-S. Ho, B. Qian, and S. Cai, J. Appl. Phys. **72**, 4469 (1992).
[99]M. Brodsky, M. Cardona, and J. Cuomo, Phys. Rev. B **16**, 3556 (1977).
[100]D. Bhusari and S. Kshirsagar, J. Appl. Phys. **73**, 1743 (1993).
[101]M. Gorman and S. Solin, Solid State Commun. **15**, 761 (1974).
[102]A.-I. El Khalfi, E. M. Ech-chamikh, Y. Ijdiyaou, M. Azizan, A. Essafti, L. Nkhaili, and A. Outzourhit, Spectrosc. Lett. **47**, 392 (2014).
[103]S. Rejeb, R. Gharbi, M. Fathallaha, F. Demichelis, C. Pirri, E. Tresso, and G. Crovini, Opt. Mater. **6**, 13 (1996).
[104]T. Stapinski, B. Swatowska, S. Kluska, and E. Walasek, Appl. Surf. Sci. **238**, 367 (2004).
[105]G. Ambrosone, D. Basa, U. Coscia, and P. Rava, Thin Solid Films **518**, 5871 (2010).
[106]M. A. Worsley, J. D. Kuntz, J. J. H. Satcher, and T. F. Baumann, J. Mater. Chem. **20**, 4840 (2010).
[107]H. Ghim Wei, W. Andrew See Weng, K. Dae-Joon, and E. W. Mark, Nanotechnology **15**, 996 (2004).
[108]J. C. Li, C. S. Lee, and S. T. Lee, Chem. Phys. Lett. **355**, 147 (2002).
[109]F. Giorgis, G. Ambrosone, U. Coscia, S. Ferrero, P. Mandracci, and C. Pirri, Appl. Surf. Sci. **184**, 204 (2001).
[110]M. Loulou, R. Gharbi, M. Fathallah, G. Ambrosone, U. Coscia, G. Abbate, A. Marino, S. Ferrero, and E. Tresso, J. Non-Cryst. Solids **352**, 1388 (2006).
[111]D. Basa, Thin Solid Films **406**, 75 (2002).
[112]K. Mui, D. Basa, F. Smith, and R. Corderman, Phys. Rev. B **35**, 8089 (1987).
[113]See supplementary material at https://doi.org/10.1116/1.5097628 for ellipsometry data analysis for SiC films using Graded layer model (or simple graded index model) (GTL), BEMA calculation, and X-ray diffraction patterns of the SiC films.